THE GEOLOGICAL SOCIETY OF AMERICA®

Successive accretions of future allochthonous terranes and multiple subduction zone jumps: Implications for Tethyan evolution

Zhiyong Yan[1], Lin Chen[1,†], Andrew V. Zuza[2], and Qingren Meng[1]

[1]*State Key Laboratory of Lithospheric Evolution, Institute of Geology and Geophysics, Chinese Academy of Sciences, Beijing 100029, China*

[2]*Nevada Bureau of Mines and Geology, Nevada Geosciences, University of Nevada, Reno, Nevada 89557, USA*

ABSTRACT

The accretion of future allochthonous terranes (e.g., microcontinents or oceanic plateaus) onto the southern margin of Asia occurred repeatedly during the evolution and closure of the Tethyan oceanic realm, but the specific geodynamic processes of this protracted convergence, successive accretion, and subduction zone initiation remain largely unknown. Here, we use numerical models to better understand the dynamics that govern multiple terrane accretions and the polarity of new subduction zone initiation. Our results show that the sediments surrounding the future terranes and the structural complexity of the overriding plate are important factors that affect accretion of multiple plates and guide subduction polarity. Wide (≥400 km) and buoyant terranes with sediments behind them and fast continental plate motions are favorable for multiple unidirectional subduction zone jumps, which are also referred to as subduction zone transference, and successive terrane-accretion events. The jumping times (∼3–20 + m.y.) are mainly determined by the convergence rates and rheology of the overriding complex plate with preceding terrane collisions, which increase with slower convergence rates and/or a greater number of preceding terrane collisions. Our work provides new insights into the key geodynamic conditions governing multiple subduction zone jumps induced by successive accretion and discusses Tethyan evolution at a macro level. More than 50 m.y. after India-Asia collision, subduction has yet to initiate along the southern Indian plate, which may be the joint result of slower plate convergence and partitioned deformation across southern Asia.

Lin Chen https://orcid.org/0000-0003-3098-7697

†chenlin@mail.iggcas.ac.cn

1. INTRODUCTION

Terrane accretion (e.g., microcontinent or oceanic plateau) plays an important role in the growth of continents and the formation of supercontinents throughout Earth's history (Fig. 1A; e.g., Şengör et al., 1988, 2018; Stampfli and Borel, 2002; Tetreault and Buiter, 2014; Wan et al., 2019). In many cases, the collision of future allochthonous terranes with the subduction system and continental margin requires a subduction zone transference to establish a new subduction system on the outboard side of the terrane (Fig. 1A; e.g., Wan et al., 2019; Wu et al., 2020; Zhong and Li, 2020; Yan et al., 2021; Yang, 2022). When the same subduction direction is maintained, this is referred to as a subduction zone jump, whereas if the subduction polarity is reversed, this is known as a subduction polarity reversal (Fig. 1A).

On a broad scale, the Tibetan lithosphere of central Asia was constructed through the successive accretion of continental ribbons (i.e., future allochthonous terranes) derived from Gondwana (Fig. 1B; e.g., Şengör et al., 1988; Stampfli and Borel, 2002; Kapp and DeCelles, 2019; Wan et al., 2019; Wu et al., 2020). Prior to their accretion, these future allochthonous terranes occupied the Tethyan oceanic realm and were separated by the Proto-, Paleo-, and Neo-Tethyan oceans. The progressive Paleozoic–Mesozoic collision of these continental ribbons against the Asian continent ultimately led to the closure of the Tethyan realm (Fig. 1B; Wan et al., 2019; Wu et al., 2020; Liu et al., 2021), which involved multiple processes of collision and subduction initiation, including subduction jumps during the collision of an early Paleozoic oceanic plateau in the Qilian Shan (e.g., Song et al., 2017) and the collision of Jurassic oceanic plateau in Qiangtang (e.g., Yan and Zhang, 2020; Zhang et al., 2021), the accretion of the Qiangtang block (e.g., Liu et al., 2021), and the closure of the Neo-Tethyan Ocean (e.g., Wan et al., 2019). Therefore, the evolution of the Tethyan realm is an ideal laboratory for studying successive terrane-accretion events and multiple phases of subduction initiation. Most of these new subduction zones induced by collisions of terranes within the Tethyan oceanic realm initiated with north-dipping subduction (Fig. 1B; e.g., Song et al., 2018; Kapp and DeCelles, 2019; Wan et al., 2019), such as the subduction zone jump induced by the collision between the Meso-Tethyan Ocean oceanic plateau and the southern Qiangtang in the Jurassic (Wan et al., 2019; Yan et al., 2021). The timing to initiate these multiple subduction zone jumps varies widely, from >30 m.y. to ∼10 m.y. (e.g., Wu et al., 2020; Yang, 2022, and references therein). This series of subduction zone jumps induced by the collision of future allochthonous terranes was referred to as the "Tethyan one-way train" (Wan et al., 2019). However, the subduction zone transference process was complex during the accretion of the Tethyan oceanic realm; in some cases, subduction was active on both sides of the future allochthonous terranes prior to terrane accretion (e.g., the Lhasa terrane; e.g., Wu et al., 2016; Kapp and DeCelles, 2019; Wan et al., 2019; Yang, 2022). This dynamic process of successive episodes of terrane accretion and the factors that control the polarity of multiple subduction initiation events, and the jumping time, are still poorly known.

Accretion and subduction zone jumps are impacted by the width and rheological structure of allochthonous terranes, the thickness of the crust, convergence rates, boundary convergence forces, mantle convection, pre-existing weak zones, rheological strength and the thermal structure of passive continental margins, and the geometry of subduction zones (e.g., Cloos, 1993; Nikolaeva et al., 2010, 2011; Marques et al., 2013, 2014; Tetreault and Buiter, 2012, 2014; Moresi et al., 2014; Vogt and Gerya, 2014; Leng and Gurnis, 2015; Wan et al., 2019; Kiss et al., 2020; Gün et al., 2021; Yan et al., 2021, 2022; Zhong and

GSA Bulletin;
published online 18 January 2024

https://doi.org/10.1130/B37263.1.

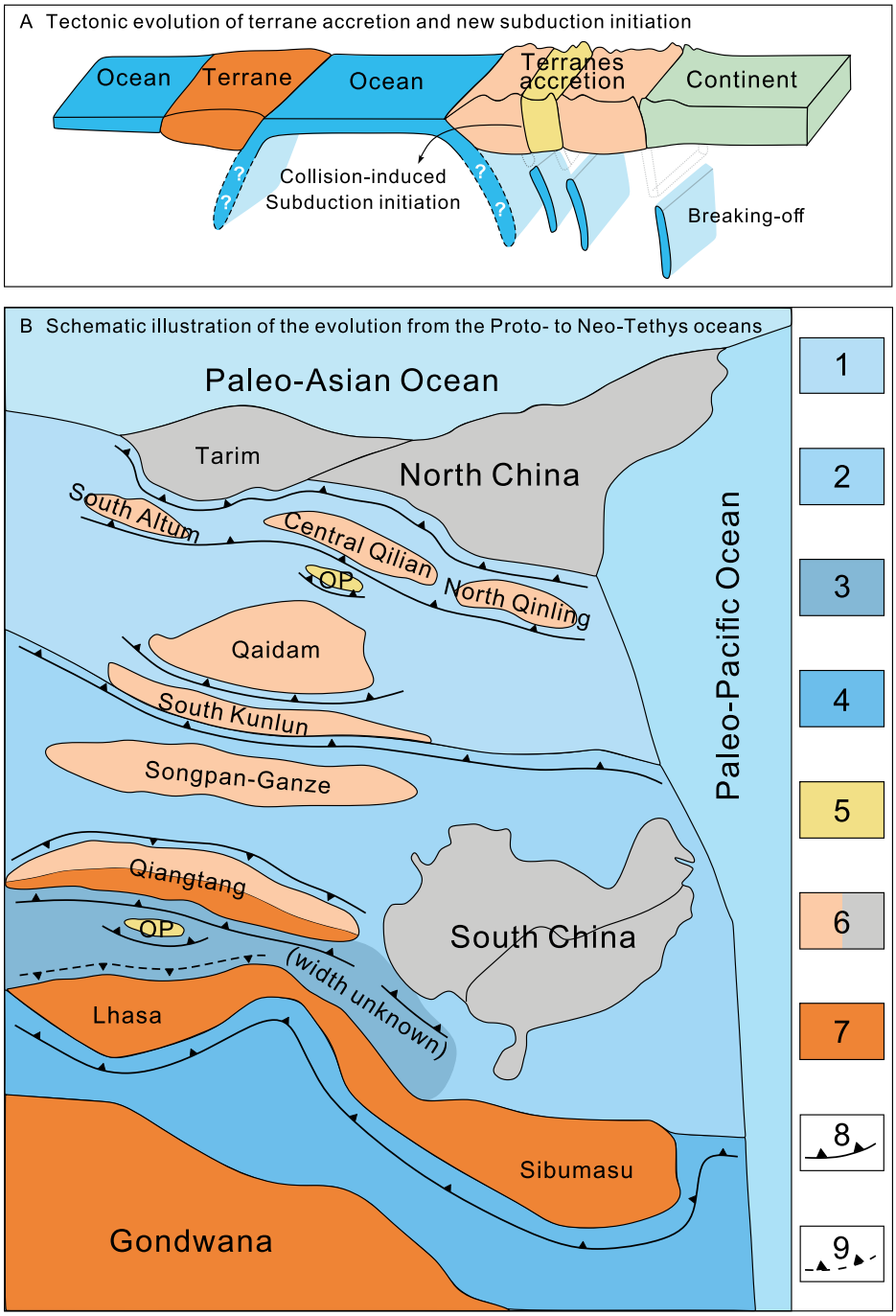

Figure 1. (A) Tectonic evolution of terrane accretion and new subduction initiation modified after Li et al. (2023). (B) Schematic illustration of the evolution from the Proto-Tethys to the Neo-Tethys oceans modified after Song et al. (2018), Kapp and DeCelles (2019), and Liu et al. (2021). 1—Proto-Tethyan Ocean; 2—Paleo-Tethyan Ocean; 3—Meso-Tethyan Ocean; 4—Neo-Tethyan Ocean; 5—oceanic plateau (OP); 6—Pan-Cathaysian continental blocks; 7—Gondwana and Cimmerian blocks; 8—subduction zone; 9—conceivable subduction zone.

Li, 2022). However, past studies only considered the dynamics of continental accretion (e.g., Moresi et al., 2014), the subduction initiation of the passive continental margin without the collision process (e.g., Marques et al., 2013, 2014), or a single phase of subduction zone jump (e.g., Yan et al., 2021). In these dynamic models, the subduction zone jump is less likely to occur, and the time from collision to subduction initiation is very short (<10 m.y.; Zhong and Li, 2020; Yan et al., 2021), which is inconsistent with the geologically observed jumping times (~10–30 + m.y.; Wu et al., 2020; Yang, 2022, and references therein). There have not yet been quantitative numerical simulations to explore the dynamic drivers and impacts of the multiple unidirectional subduction zone jumps. At the same time, few works have considered the role of the depleted mantle of future allochthonous terrane (e.g., Kerr, 2014; Scott et al., 2014; Mochizuki et al., 2019), which is a very important factor since the lateral contrast of density and strength between the oceanic plateau and the normal oceanic lithosphere offers a logical location for the formation of a weakness zone favoring subduction initiation (Abbott and Mooney, 1995; Niu, 2018; Yan et al., 2021).

Previous studies suggested that the sedimentary loads and the resulting rheological weakening can affect the dynamics in subduction zones (Cloetingh et al., 1982; Gerya and Meilick, 2011; Brizzi et al., 2020, and references therein). A large number of geological, geophysical, and experimental observations showed that subducting sediments have weak friction and/or exhibit high-pore fluid pressure, thereby reducing the inter-plate coupling force and changing the subduction speed (e.g., Kopf and Brown, 2003; Bangs et al., 2009; Tobin and Saffer, 2009; Behr and Becker, 2018). Previous studies argued that the tropical latitudes could have favored the deposition of sediments on the Tethyan seafloor (Hoareau et al., 2015, and references therein). Interestingly, recent plate reconstruction results also imply a correlation between the acceleration of the Indian plate and the arrival of Tethyan equatorial sediments at the subduction trench (Behr and Becker, 2018). What role, then, do sediments around future allochthonous terranes play in the initiation of subduction after the collision?

In this study, based on our previous model of a single subduction zone jump (Yan et al., 2021, 2022), we designed new numerical models to explore the dynamics of successive accretions and multiple episodes of subduction initiation induced by future allochthonous terranes. We numerically investigated the end-member case where the multiple collisions of future allochthonous terranes onto the continental margin lead to outward multiple subduction zone jumps, focusing on the multiple collisions and subduction process and the factors controlling the polarity of subduction initiation and the jumping time. First, we systematically tested possible influencing factors, including sediments, convergence rates, and properties of future allochthonous terranes (width and depleted mantle). Next, we compared the geologic history of the Tethyan tectonic domain, including the main structural units and suture zones, to our model results. Our results provide new insights into the dynamic growth of the Tethyan system,

and also shed light on the dynamics of multiple episodes of collisional accretion and subduction initiation, as well as supercontinent formation.

2. METHODS

The 2-D thermomechanical numerical model based on the code I2VIS (Gerya and Yuen, 2003) has a width of 8000 km and a depth of 1000 km with a Euler grid of 1461 × 271 (Fig. 2A). This code is based on the finite-difference method with the marker-in-cell technique to solve the governing equations of conservation of momentum, mass, and energy, and the detailed numerical methods and physical parameters are shown in the Supplemental Material[1]. The continental and oceanic plates are configured on the left and right sides of the model, respectively, and the three identical future allochthonous terranes are equidistantly embedded in the ocean. We use the future allochthonous terranes to represent exotic buoyant geologic units, such as microcontinents or oceanic plateaus, which collide with the continental plate in our models (e.g., Tetreault and Buiter, 2014). We developed and tested a total of 39 sets of models to study multiple episodes of accretion and subduction initiation (Table 1). First, we established end-member models under four different conditions (Fig. 2D) to examine the role of sediments, including models with sediments only on the right side of the future allochthonous terranes (Model 1, Figs. 3 and 4), sediments on both sides of the future allochthonous terranes (Model 2), sediments only on the left side of the terranes (Model 3, Fig. 5), and no sediments surrounding the terranes (Model 4). The convergence rates of the left (X = 2000 km) and right (X = 5500 km) plates in all models are 5.0 cm/yr and 5.0 cm/yr, respectively, with a total convergence rate of 10 cm/yr. The widths of the three future allochthonous terranes in these models are 500 km, the thickness of the crust is 30 km, and the density is 2850 kg/m^3. These values are within the range of modern oceanic plateaus, microcontinents, and island arcs (Tetreault and Buiter, 2014). Subsequently, we designed 16 sets of convergence-rate comparison models and 19 sets of tests on the buoyancy properties (i.e., width and mantle lithospheric density) of future allochthonous terranes. The plate convergence rate ranges from 4 cm/yr to 10 cm/yr, and the width and mantle-depleted density ($\Delta\rho$) range from 200 km to 600 km and 0 kg/m^3 to 70 kg/m^3, respectively. More details of the models are shown in Table 1. Depleted density ($\Delta\rho$) refers to the difference in the lithospheric density of the oceanic mantle compared to that of future allochthonous terrane mantle.

[1]Supplemental Material. Text S1, Tables S1 and S2, Figures S1 and S2, and Videos S1–S5, including the numerical methods and model setup, the material properties used in the numerical experiments, the composition and density field in Model 1 at 31.8 m.y., the evolution of the composition in Model 6, and animated evolutions of the main models are described. Please visit https://doi.org/10.1130/GSAB.S.24650208 to access the supplemental material, and contact editing@geosociety.org with any questions.

3. MODEL RESULTS

3.1. Influence of Sediments

Model 1, with sediments only on the right side of the future allochthonous terranes, results in a one-way, multiple-subduction-zone jump process (Fig. 3). First, the oceanic plate initially subducted with a shallow angle, and then the first terrane collided with the trench and accreted on the continental margin, and the slab steepened as

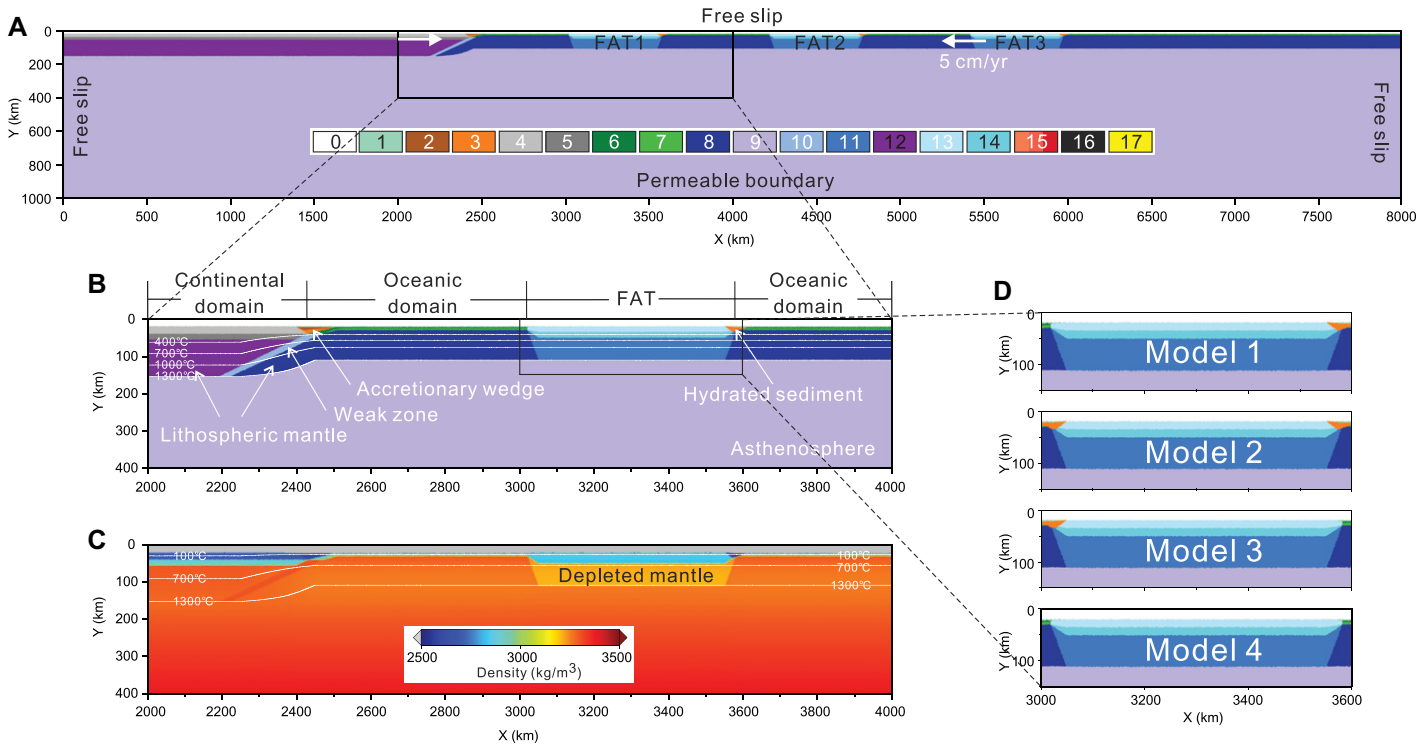

Figure 2. (A) Model setup of the compositional field of the reference model. FAT—future allochthonous terrane. (B and C) Enlargement of the area of interest showing the detailed structure of composition, density, and temperature. White solid lines denote isotherms. (D) Partial enlarged view of the allochthonous terrane of the Models 1–4. Composition color codes: 0—stick air; 1—water; 2 and 3—sediments; 4 and 5—continental upper and lower crust; 6 and 7—oceanic upper and lower crust; 8—oceanic lithosphere; 9—asthenospheric mantle; 10—hydrated mantle; 11—FAT (depleted) lithosphere; 12—continental mantle; 13 and 14—FAT upper and lower crust; 15—partially molten oceanic/FAT crust and partially molten mantle; 16—eclogitization of oceanic/FAT crust; 17—serpentinized mantle.

TABLE 1. NUMERICAL MODELING EXPERIMENTS

Model	Sediment location	Velocity (cm/yr)		Properties of FAT		Figure(s)
		V_C	V_O	Width (km)	$\Delta\rho$ (kg/m^3)	
Model 1	Right	5	5	500	50	Figs. 3, 6
Model 2	Both					—
Model 3	Left					Fig. 5
Model 4	No					—
M-v1	Right	5	4	500	50	Fig. 6
M-v2		5	3			Fig. 6
M-v3		5	2			Fig. 6
M-v4		4	5			Fig. 6
M-v5		4	4			Fig. 6
M-v6		4	3			Fig. 6
M-v7		4	2			Fig. 6
M-v8		3	5			Fig. 6
M-v9		3	4			Fig. 6
Model 5		3	3			Figs. 6, 7
M-v10		3	2			Fig. 6
M-v11		2	5			Fig. 6
M-v12		2	4			Fig. 6
M-v13		2	3			Fig. 6
Model 6		2	2			Figs. 6, S1†
Model 7		5*	5*			Fig. 7
M-p1	Right	5	5	600	70	Fig. 6
M p2				600	50	Fig. 6
M-p3				600	30	Fig. 6
M-p4				600	0	Fig. 6
M-p5				500	70	Fig. 6
M-p6				500	30	Fig. 6
M-p7				500	0	Fig. 6
M-p8				400	70	Fig. 6
M-p9				400	50	Fig. 6
M-p10				400	30	Fig. 6
M-p11				400	0	Fig. 6
M-p12				300	70	Fig. 6
M-p13				300	50	Fig. 6
M-p14				300	30	Fig. 6
M-p15				300	0	Fig. 6
M-p16				200	70	Fig. 6
M-p17				200	50	Fig. 6
M-p18				200	30	Fig. 6
M-p19				200	0	Fig. 6

Note: V_C—velocity of continental plate; V_O—velocity of oceanic plate; FAT—future allochthonous terrane; $\Delta\rho$—the difference in the lithospheric density of the oceanic mantle compared to that of future allochthonous terrane mantle.

*The additional convergence rate imposed on the plate ceases after 50 m.y.

†See text footnote 1.

the subducted length of slab increased, accompanied by partial melting of the subducted oceanic crust (Fig. 3A; Video S1). After the frontal slab broke off, a new subduction zone formed to the right of the first terrane, which allowed continuous convergence (Fig. 3B). The detached slab subducted into the asthenosphere and stagnated at a depth of ~660 km, which was determined by the difference between the density of the subducting slab and the density of the surrounding asthenospheric material (Fig. S1). The first subduction zone jump, shown in panels A and B (Fig. 3), occurred ~2.8 m.y. after terrane collision and accretion, which we consider to be the time for a subduction zone jump (Fig. 4A). As the ocean closed between the two terranes, the second terrane collided with the first one, and then a second subduction zone initiated behind the second terrane (Figs. 3C and 3D). Similarly, after the subduction of the oceanic slab was completed, the third terrane collided with the second one, and the third subduction zone started to form on its right side (Figs. 3E and 3F). Interestingly, after the terrane collision and before new subduction started, the subducted frontal slabs broke off, and then the two detached slabs finally stagnated at ~660 km like the first slab (Fig. S1). These two processes are the subduction zone jumps that were induced by the collision of the second and third terranes. The times of the second and third subduction zone jumps are ~3.6 m.y. and 8.2 m.y., respectively (Fig. 4A).

After successive collisions between future allochthonous terranes and continental margin or previous terrane, a new subduction initiation occurs, triggering the multiple subduction zone jumps, and magmatic activity migrates away from the continent (Figs. 3, 4B, and 4C). Every time the subduction zone jumps, it is also accompanied by a change of the overriding plate tectonic force measured at X = 2100 km (Fig. 4A), which provides a unique time for marking the onset of a subduction-jump time. Tectonic force is defined as the integral of the horizontal deviatoric stress along the vertical direction of lithosphere, which describes the stress state inside the lithosphere. The stress of the overriding plate drops suddenly due to the subduction initiation, increase of the subduction angle, breakoff of subducted slab, or trench retreat, but it does not change from compression to tension. The completion of each subduction cycle corresponds to a sharp switch of the tectonic force from tension to compression (Fig. 4A).

The evolution of Model 2, with sediments on both sides of the future allochthonous terranes, is similar to that of Model 1, and the times of the multiple subduction zone jumps are ~3.4 m.y., 5.3 m.y., and 8.2 m.y., respectively (Video S2). However, Model 3, with sediment on the left side, and Model 4, without sediment around the future allochthonous terranes, have different evolutionary processes than Model 1 (Fig. 5; Videos S3 and S4). After the first terrane collided (Fig. 5A), the polarity of the oceanic plate behind it reversed and subducted to the right along the sediment (Figs. 5B and 5C). When the second terrane collided with the first one, the oceanic slab subducted to the left again, rather than on the sediment side (Fig. 5D). After the third terrane collided with the second one (Fig. 5E), a third phase of subduction initiated on its right side (Fig. 5F). Model 3 and Model 4 did not undergo multiple subduction zone jumps, but multiple subduction polarity reversals did occur (e.g., Fig. 5).

3.2. Influence of Convergence Rates and Properties of Terrane

Here, we systematically test the convergence rate (Fig. 6A) and the properties of future allochthonous terranes (width and depletion degree of the mantle; Fig. 6B) because the plate convergence rate has an important influence on the subduction zone (e.g., Lallemand et al., 2005; Yan et al., 2022), and different oceanic plateaus can reorganize subduction zones (Yan et al., 2021). All of the models are compared to reference Model 1, and the results are summarized in Figure 6.

When the velocity of the overriding plate is greater than or equal to 2 cm/yr and greater than or equal to the velocity of the oceanic plate, the model undergoes multiple subduction zone jumps (Fig. 6A). The jumping time of the three subduction-zone jumps in the same model gradually increases, whereas the jump time decreases with an increase of convergence rates in different models (Fig. 6C). The difference is that after the last terrane collision of Model 6, there is no obvious subduction initiation for a long time (~30 m.y.; Fig. S1 and Video S5). When the width of the future allochthonous terrane is <500 km, only sporadic models experience multiple subduction zone jumps (Fig. 6B).

Furthermore, we tested the impact of time-varying convergence rate on subduction initiation and jumps. The settings of Model 5 and Model 7 are the same. The left and right boundaries are

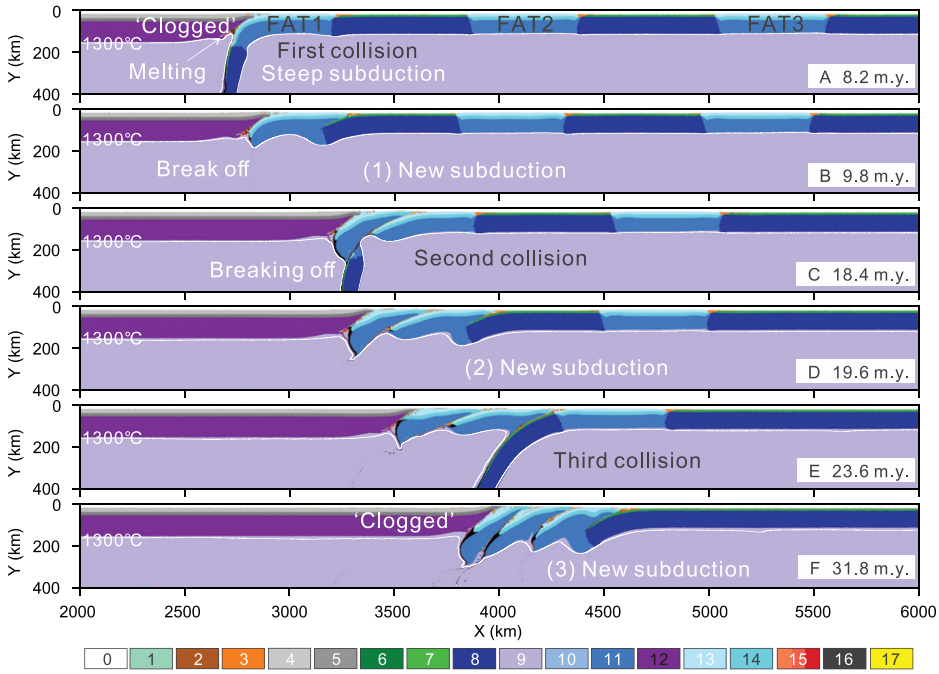

Figure 3. Evolution of composition in reference Model 1. FAT—future allochthonous terrane. White solid lines denote isotherms. Composition color codes: 0—stick air; 1—water; 2 and 3—sediments; 4 and 5—continental upper and lower crust; 6 and 7—oceanic upper and lower crust; 8—oceanic lithosphere; 9—asthenospheric mantle; 10—hydrated mantle; 11—FAT (depleted) lithosphere; 12—continental mantle; 13 and 14—FAT upper and lower crust; 15—partially molten oceanic/FAT crust and partially molten mantle; 16—eclogitization of oceanic/FAT crust; 17—serpentinized mantle.

free-slip, as with those of Model 1 (Table 1), and the additional initial velocities imposed on the continental and oceanic plates are both 3 cm/yr (Fig. 7). However, the additional convergence rate imposed on the plate in Model 7 ceases after 50 m.y., leaving only free slip boundaries (Fig. 7B2), whereas the Model 5 plate maintains continuous convergence (Fig. 7A2). Before 50 m.y., Model 5 and Model 7 had an evolution process similar to that of Model 1, and three terranes with positive buoyancy were blocked at the trench (Figs. 7A2 and B2). After 56.6 m.y., Model 5, with continuous convergence, had new subduction initiation behind the third terrane and experienced a new subduction zone jump (Figs. 7A3 and B4). However, in Model 7, the terranes were blocked in the trench, and the oceanic plate behind them had not undergone new subduction after 50 m.y. (Fig. 7B).

4. DISCUSSION

4.1. Controlling Factors and Jumping Time of Multiple Subduction Zone Jumps

Sustained convergence influences the occurrence of multiple subduction zone jumps (Fig. 7). Because of the numerous slab detachments during accretion, there is no dense subducting slab to sustain subduction after the collision (Fig. 7B), and new subduction initiation requires the action of an external force (e.g., Li et al., 2023). Here, we exert a sustained convergent force that induces post-collision subduction zone jumps (Fig. 7A). Our results suggest that an overriding plate with a velocity greater than or equal to that of the oceanic plate favors the formation of multiple subduction zone jumps accompanied by slab break-off (Fig. 6A). The depleted mantle of the future allochthonous terranes increases their buoyancy and also results in a significant difference in material and viscosity between the terrane and oceanic plate, which is conducive to the break off of the frontal slab, the coupled blockage of the terranes in the subduction zone, and a subduction zone jump at the terrane-ocean boundary (e.g., Figs. 2, 7, and 8). This finding is similar to the results of Tao et al. (2020) and Yan et al. (2021). However, Zhong and Li (2020) argued that small terranes are more likely to trigger subduction zone jumps than large terranes, although their models only considered single terrane collisions and a single phase of subduction zone jump. Furthermore, our new results show that multiple subduction zone jumps require wider terranes (≥400 km) than a single-sequence subduction zone jump (~300 km in Yan et al., 2021). Our new results suggest that collisions of large terranes with depleted mantle can trigger subduction initiation with slab detachment under successive convergences, but the polarity of subduction can vary (Fig. 8).

The sediment around the future allochthonous terranes promotes and guides subduction polarity (e.g., Figs. 3 and 8), but this is not the only absolute factor for multiple jumps of the subduction zone (e.g., Figs. 5 and 8). After the first terrane collision, the oceanic plate between the first and the second terrane experienced contractional deformation under continued compression. At this time, the rheological strengths of the two terranes were similar, and sediment played a major role in guiding the initiation of subduction (Figs. 8A1 and 8B1) along the side with sediments (Figs. 8A2 and 8B2). However, after the collision of the second terrane, the direction of subduction initiation did not occur along the location of the sediment, because the complex region of the first and second terrane on the left side of the oceanic plate was weaker, resulting in a larger lateral difference (Figs. 8A3 and 8B3). In Model 1, the sediment and the terrane complex were on the same side of the oceanic plate, which further promoted the weakening of the contact zone, and the subduction initiated with the same polarity (Fig. 8A4). In Model 3, the stress of the oceanic plate accumulated near the second terrane side rather than the sediment side (Fig. 8B3), so new subduction initiated in a weaker direction than the sediment side (Fig. 8B4). Therefore, the sediment around the terranes can promote subduction initiation, which may induce polarity reversal of subduction, but the patchwork complex of accreted terranes is often more likely to be compressed and deformed to cause stress cumulation, which induces subduction initiation of the subsequent oceanic plate (Fig. 8). The lateral viscosity difference around the terranes determines where the subduction initiates. Thus, we believe that the collage of multiple terranes is often accompanied by subduction initiation in the same direction, and polarity reversals of subduction may also occur due to the role of sediment.

Figure 6C summarizes the jumping time of multiple subduction zone jumps for different models. As the convergence rate increases, the jumping time of the subduction zone jump gradually decreases. In the same model, the time of the later subduction zone jump is longer than that of the previous subduction zone jump, which is a trend in all models. The time of the third subduction zone jump is significantly longer than that of the first one (Fig. 6C). The timing of the third subduction zone jump in most

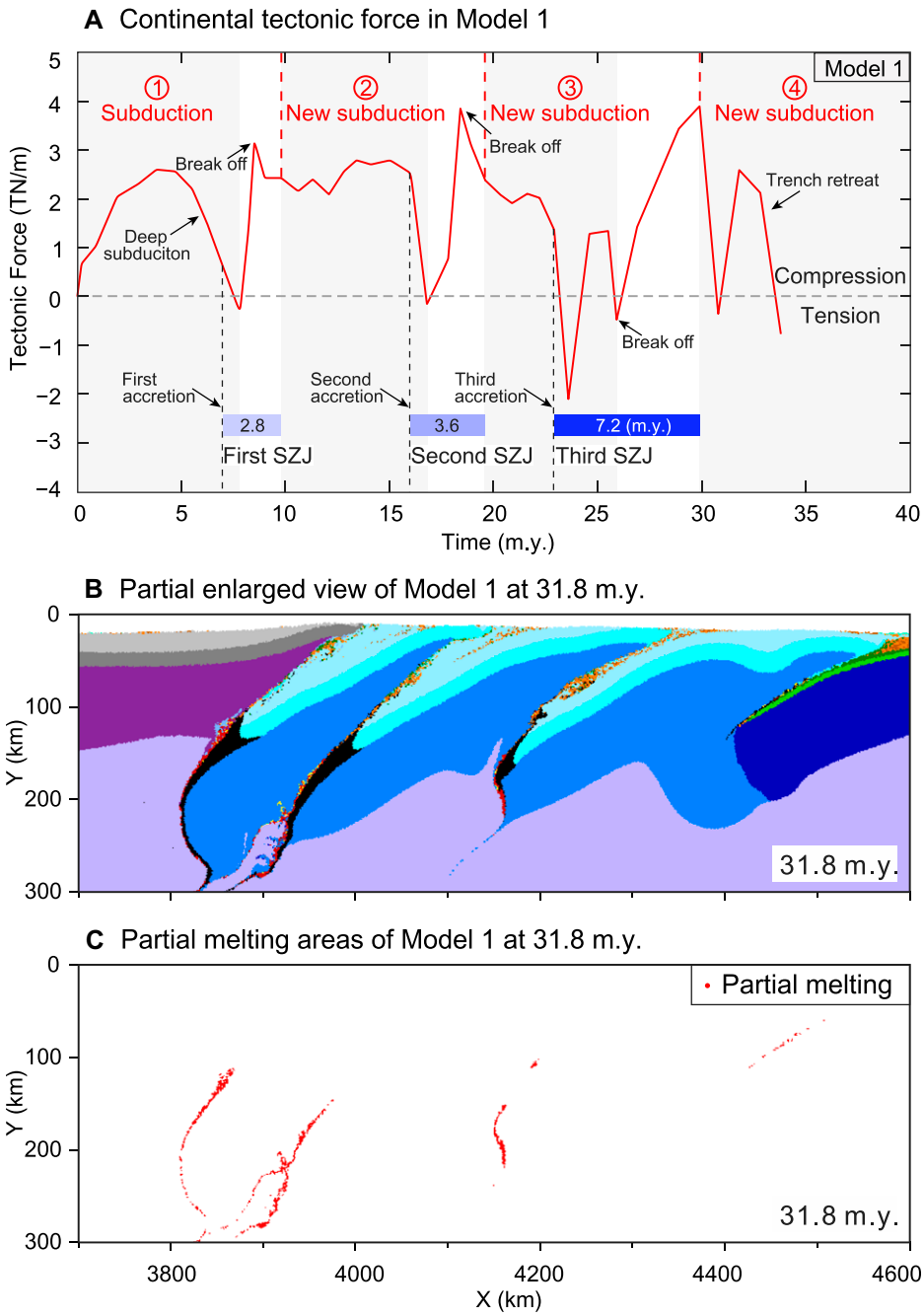

Figure 4. (A) Evolution of continental tectonic force (X = 2100 km) with time for reference Model 1, which reflects the different stages of model evolution. SZJ—subduction zone jump. Gray area is the duration of each full subduction. Blue bars represent the three jumps and their jumping time. (B) Partial enlarged view of the compositional evolution of Model 1 at 31.8 m.y. Composition color code shown in this figure is the same as in Figures 2, 3, and 5. (C) Only partial melting of Model 1 at 31.8 m.y. is shown.

models exceeds 10 m.y. (red circles in Fig. 6C; ~10–20 m.y.), which differs from the results of previous modeling studies (Zhong and Li, 2020; Yan et al., 2021). This effect is caused by the protracted accretion of allochthonous terranes that were continually shortened during plate convergence, and thus strain was partitioned into this accretionary complex. For example, the complex was shortened by ~800 km during the ~30 m.y. history of the model with multiple subduction zone jumps (Fig. 3). This process slows stress buildup between the terrane complex and the oceanic slab to initiate new oceanic subduction (Figs. 3 and 8A). For a prolonged period of time after the collision and before the new subduction, the stress is absorbed by the terrane complex, so that the more terranes in the complex, the longer the time required for the later subduction zone jump (Fig. 6C). This terrane complex with weak suture zones readily absorbs shortening (e.g., Chen et al., 2017, 2020; Liu et al., 2023). Our model predicts that the time required for the onset of new subduction induced by collisions is primarily governed by the convergence rates and strength of the overriding continental plate of the complex (the successive accretion of future allochthonous terranes onto the continental plate). It is harder for new subduction zones to form after multiple terrane collisions or if the convergence rates become too low.

4.2. Comparison with Previous Simulation Results

Previous numerical modeling studies explored the accretion, subduction initiation, and flat-slab subduction processes of future allochthonous terranes (e.g., Marques et al., 2014; Moresi et al., 2014; Vogt and Gerya, 2014; Zhong and Li, 2020; Yan et al., 2021, 2022). They systematically studied single-collision accretion processes (e.g., Tetreault and Buiter, 2012) and/or subduction zone jumps (e.g., Yan et al., 2021) and subduction polarity reversals (e.g., Sun et al., 2021). These numerical simulations furthered our understanding of the geodynamic processes of collision and subduction initiation, but none reproduced the multiple terrane-accretion events envisioned for the Wilson Cycle and supercontinent formation, including evolution of the Tethyan realm (Wu et al., 2016; Kapp and DeCelles, 2019).

Our new models show, for the first time, a multi-cycle process from collision to accretion to new subduction initiation (e.g., Fig. 3). The lateral heterogeneity between the terranes and the surrounding oceanic lithosphere favors accretion, slab detachment, and subduction zone jump, which is consistent with previous results (e.g., Zhong and Li, 2020; Yan et al., 2021). However, our new results reveal that more complexity is involved in identifying the location and polarity of new subduction initiation during terrane accretion, with influence by sediments, convergence rate, and previous terrane-accretion events. That is to say, the conditions and results of a single subduction zone jump may not be scalable for predicting multiple subduction zone jumps. Moreover, the estimated time from collision to subduction initiation was very short (<10 m.y.) in the previous studies (Zhong and Li, 2020; Yan et al., 2021), which is inconsistent

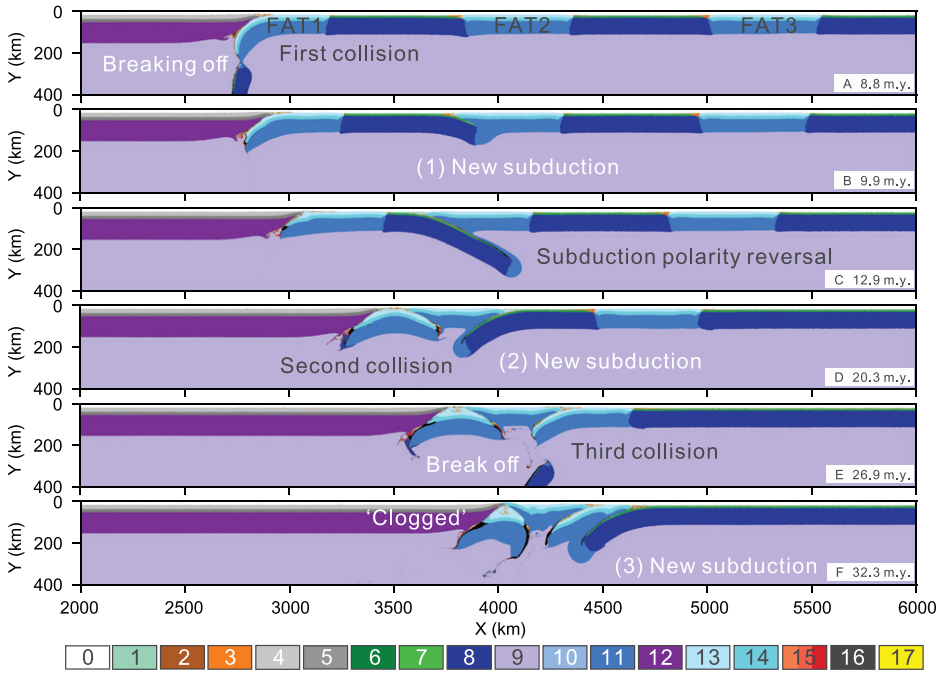

Figure 5. Evolution of composition in reference Model 3. FAT—future allochthonous terrane. Composition color codes: 0—stick air; 1—water; 2 and 3—sediments; 4 and 5—continental upper and lower crust; 6 and 7—oceanic upper and lower crust; 8—oceanic lithosphere; 9—asthenospheric mantle; 10—hydrated mantle; 11—FAT (depleted) lithosphere; 12—continental mantle; 13 and 14—FAT upper and lower crust; 15—partially molten oceanic/FAT crust and partially molten mantle; 16—eclogitization of oceanic/FAT crust; 17—serpentinized mantle.

with some of the geologically observed jumping times (~10–30 + m.y.; Wu et al., 2020; Yang, 2022, and references therein). Our new results show that the jumping time (~3–20 + m.y.) is related to the convergence rates and the overriding plate comprised of accreted terranes, which provides a possible explanation for geological observations of longer jump times.

4.3. Implications for Tethyan Dynamics

During the Phanerozoic period, the Tethyan oceanic realm was a complex system of oceanic lithosphere, continental terranes, and oceanic and continental arcs bounded by the Laurasia supercontinent in the north and the Gondwana supercontinent in the south (Wan et al., 2019; Wu et al., 2020). A large number of future allochthonous terranes is hypothesized to have continuously rifted from the Gondwana supercontinent in the south, thus forming the Proto-, Paleo-, and Neo-Tethyan oceans (Fig. 1B; Şengör et al., 1988; Stampfli and Borel, 2002; Kapp and DeCelles, 2019; Wan et al., 2019; Wu et al., 2020, and references therein). After a long evolution, the continental terranes and some buoyant oceanic plateaus (e.g., Proto- and Meso-Tethyan oceanic plateaus) between these oceans gradually drifted toward and collided with the Laurasia supercontinent in the north (e.g., Stampfli and Borel, 2002; Wan et al., 2019; Wu et al., 2020; Yan and Zhang, 2020; Zhang et al., 2021; Yang, 2022, and references therein).

The tectonic history of terrane drifting, subduction initiation, collision, and oceanic closure is relatively complex, but in general, continental terranes and oceanic plateaus migrated northward to collide against the Eurasian continent. Our results provide new insights into this process of progressive terrane accretion. We synthesized the major subduction and oceanic closure events along the main sutures across Tibet (e.g., the Kunlun, Jinsha, Bangong, and Indus-Yarlung suture zones, from north to south; Figs. 9A and 9B) as shown in Table 2 (e.g., Kapp et al., 2003; Wu et al., 2016; Kapp and DeCelles, 2019; Wan et al., 2019; Liu et al., 2021). We also summarized two oceanic plateau collision events in the Qilian Shan and Qiangtang regions of Tibet (Table 2), which likely behave similarly to microcontinent collision events (e.g., Tetreault and Buiter, 2014).

We first compare our models to the oceanic plateau collisions, which are relatively simple single-jump events. In the early Paleozoic Qilian Ocean, an oceanic plateau collided with the Qilian terrane at ca. 470 Ma, and a new subduction system was established outboard of this collision by 460–440 Ma (e.g., Song et al., 2017; Yang, 2022). This implies a subduction-jump time of 10–20 m.y. (Table 2), which is comparable to that of our models (Fig. 6C). Similarly, in the Qiangtang area, an oceanic plateau in the Meso-Tethyan Ocean collided with the Qiangtang continent at ca. 175 Ma, with a new subduction zone established on the outboard side of this collision by ca. 165 Ma (Yan and Zhang, 2020; Zhang et al., 2021). This implies a subduction-jump time of 10 m.y. (Table 2).

The overall closure history of the Paleo-, Meso-, and Neo-Tethyan oceans is more complicated, but our models can reproduce aspects of the successive accretion of future allochthonous terranes (Fig. 9C). Model 3, with sediment on the left side, matches the course and polarity of the subduction of these four sutures (Fig. 5). Although there may be multidirectional subduction of back-arc basins or southward subduction in some areas of Tethys, this will not change the overall northward evolution of Tethys (e.g., Wan et al., 2019). The entire Tethyan region as a whole shows a dynamic process of multiple subduction zone jumps, which has been referred to as the Tethyan one-way train (Wan et al., 2019). Subduction-related magmatic arc activity also migrated to the south (Wan et al., 2019; Yang, 2022, and references therein). Our end-member model results recreate the broad processes of multiple subduction zone jumps (e.g., Fig. 3). Along with the process of multiple subduction zone jumps, the Eurasian continental stress changed from compression to extension many times (Figs. 4A and 9C), and the magmatic activity also migrated away from the Eurasian continent (e.g., Fig. 4C). Multiple subduction zone jumps induced by successive collision of terranes can explain the first-order dynamic process of Tethys.

The accretion of most terranes occurred along a north-dipping subduction zone, which implies multiple northward subduction zone jumps. The subduction-zone jump times for the various paleo-subduction systems varied greatly. For example, the jump time after the closure of the Paleo-Tethys was rapid (<10 m.y.), as was the subduction jump timing associated with the collisions of oceanic plateaus (≤20 m.y.; Table 2). These rapid subduction zone jumps were well presented in previous models (e.g., Zhong and Li, 2020; Yan et al., 2021). However, recent geologic syntheses show that the average jumping time of subduction zone jumps in the Tethyan oceanic realm is ~10–30 m.y. (Yang, 2022), and even up to ~60 m.y., as we show for the closure of the Proto-Tethys Ocean (Table 2). These more variable and longer jump times

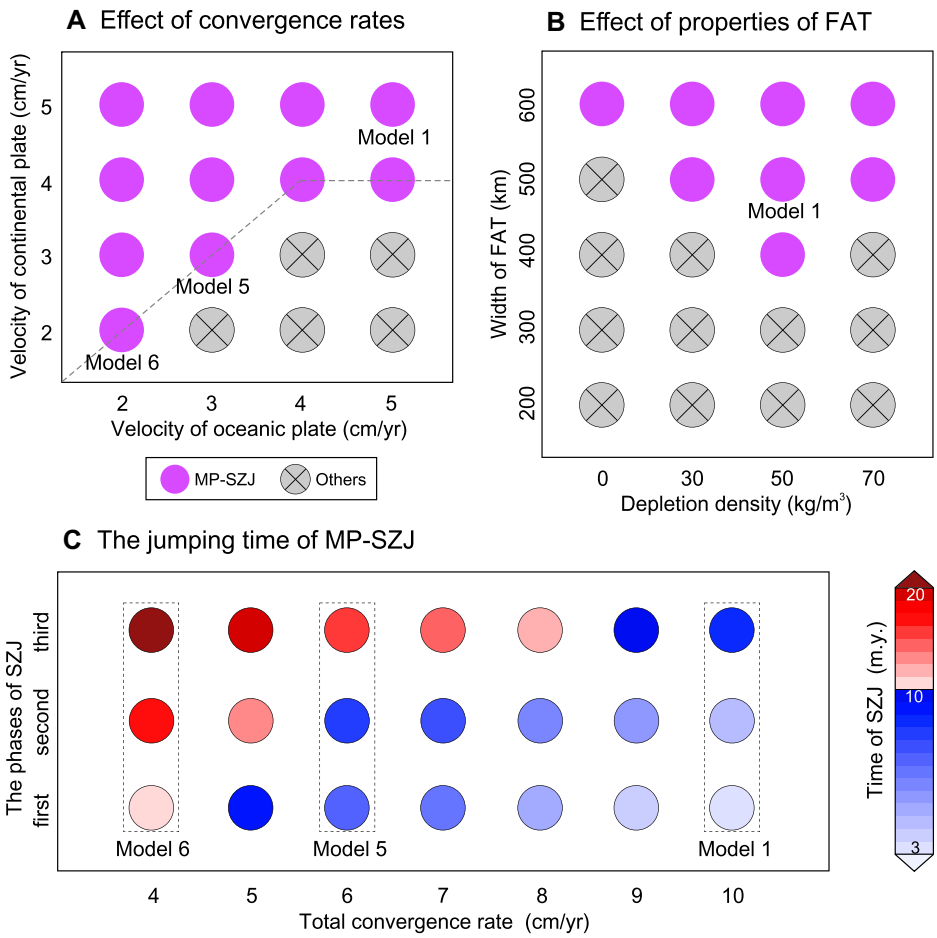

Figure 6. Summary of model results. (A) Effect of convergence rates. (B) Effect of the width and depleted mantle of future allochthonous terrane. Purple circles represent multiple subduction zone jumps. (C) Times of multiple subduction zone jumps vary with convergence rate; the time of the third subduction zone jump in Model 6 is infinite. FAT—future allochthonous terrane; MP-SZJ—multiple subduction zone jumps.

were insufficiently explained by previous models (e.g., Zhong and Li, 2020; Yan et al., 2021). Our new results provide a possible explanation: lower plate convergence rates and the patchwork complex of the terranes that collided may have played a role in this lag of subduction initiation. For example, the northern region of the Tibetan plateau experienced significant contractional deformation in the Cretaceous, with field observations suggesting as much as 35% shortening strain at this time, which is interpreted to be a far-field response to the collision between Lhasa and the southern Qiangtang terranes to the south (Wang et al., 2022). Our model results predict this process. In Model 1, after the three terranes collided with the overriding plate, but before new subduction initiated, the composite continental plate was in a state of compression (Fig. 4A) that shortened significantly far into the plate interior (Fig. 3E). Wang et al. (2022) also documented a switch from Cretaceous contraction to late Early Cretaceous extension that can be interpreted here as the onset of new subduction releasing compressional forces in the overriding plate (Fig. 4A). Our models provide new dynamic explanations for the complex geology observed across the Tibetan lithosphere.

Perplexingly, the Indian oceanic plate has not initiated a new subduction zone yet, nearly ~60 m.y. after the India-Eurasia collision (e.g., Stern, 2004; DeCelles et al., 2014; Yin and Harrison, 2000; Stern and Gerya, 2018). This may be due to continuous distributed shortening across the Tibetan plateau and southern Asia, the nature of the Indian plate, and the lack of pre-existing weak zones (Cloetingh et al., 1989; Stern and Gerya, 2018; Zhong and Li, 2020). Our model results provide new insights into this. The multi-stage closure of the Tethyan Ocean led to the successive collage of the terranes and formation of multiple sutures, such as the Indus-Yarlung, Bangong, Jinsha, and Kunlun suture zones (Figs. 1, 9A, and 9B). During the convergence of India-Eurasia, these naturally weak regions were prone to focus deformation (Clark, 2012; Yakovlev and Clark, 2014; Ingalls et al., 2016; Chen et al., 2017; Zuza et al., 2018, 2019; Li et al., 2020; Xie et al., 2021; Wang and Barbot, 2023). Crustal shortening due to India-Asia convergence is accommodated across the Himalayan-Tibetan orogen, with total shortening estimates in the ~1000–2000 km range (e.g., Yakovlev and Clark, 2014; Ingalls et al., 2016; Liu et al., 2023). Our modeling results also predict significant shortening of the patchwork complex of accreted terranes during multiple collisions, such as the ~800 km of shortening that occurred in Model 1 (Fig. 3). Therefore, India-Asia plate convergence was partitioned into the Himalaya and the coupled fold-thrust belts to the north. Geodetic and field observations show that India-Asia convergence is accommodated at uniform strain rates across the Himalayan-Tibetan orogen for ~2000 km into the Asian plate interior to the north (e.g., Clark, 2012; Zuza et al., 2020). Such strain partitioning into the continental interior helps suppress subduction initiation, as observed in Model 6 and Model 7 with low or no velocity. It is possible that after enough convergence, strain hardening in the continental interior would lead to the breaking of the plate boundary and initiation of subduction (e.g., Model 1, with a total convergence rate of 10 cm/yr). In addition, the India-Asia convergence rate has progressively slowed from >12 cm/yr to ~4 cm/yr today (Molnar and Stock, 2009; Copley et al., 2010). Therefore, we argue that distributed deformation across the Tibetan lithosphere and lower plate convergence rates are responsible for the absence of new subduction initiation in the Indian Ocean for >50 m.y. after the initial India-Eurasia collision. It is possible that progressive sediment accumulation around the southern margin of India (e.g., Sebastian et al., 2019) may facilitate future subduction initiation due to far-field forces (e.g., oceanic ridge or mantle plume). This highlights a complex cycle that is outside the scope of our study, where terrane collision, uplift, and erosion may lead to sedimentation around the colliding terrane to ultimately help initiate a new subduction zone.

5. MODEL LIMITATIONS

The evolution of the Tethyan system and closure of the Tethyan oceans was a complex process that proceeded throughout the Phanerozoic. It is impossible for a two-dimensional numerical model to reproduce this process completely, so

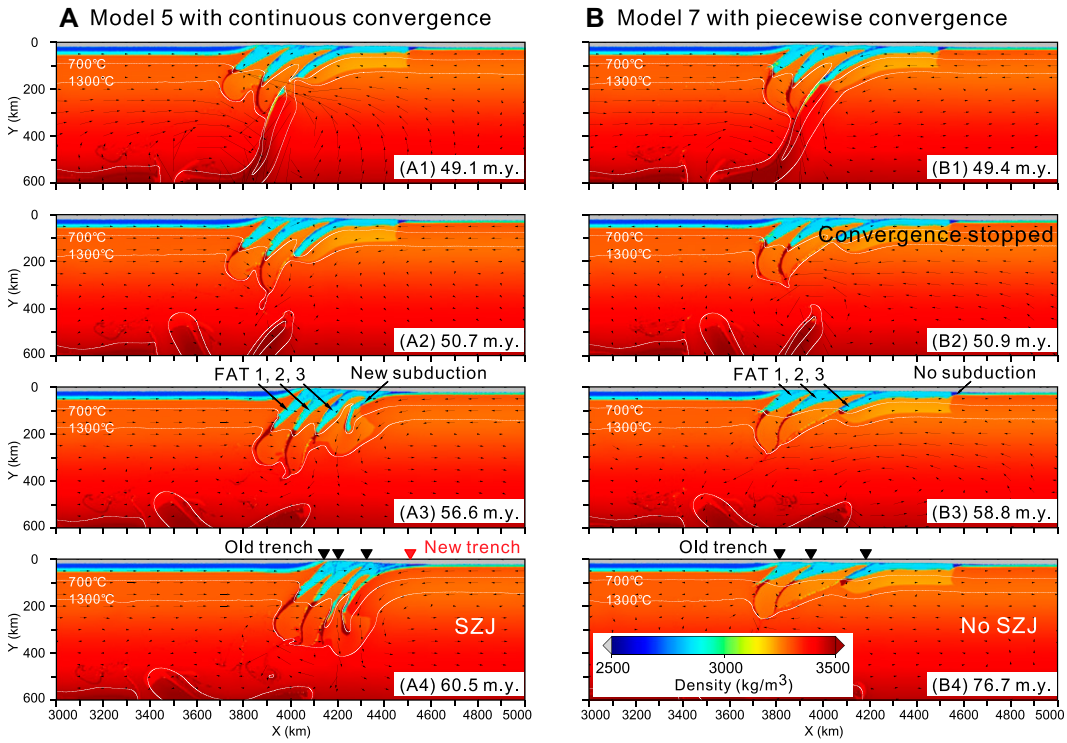

Figure 7. Evolution of density and velocity fields for models with different velocity boundary conditions. Model 5 (A) and Model 7 (B) are identical to Model 1, except that the initial velocities for the continental and oceanic plates both are 3 cm/yr. Constant plate velocities are used in Model 5, while plate velocities stop after 50 m.y. of convergence in Model 7. Solid lines with black arrows represent the velocity field, and the length of the solid line represents the relative magnitude of the velocity. FAT—future allochthonous terrane; SZJ—subduction zone jump.

our model was simplified to reasonably highlight the key points of our research.

First, since we focus on the process of multiple terrane collisions and accretion events, we did not consider the process of rifting, because it does not comprise complete evolution of the Tethyan domain. Second, limited to the two-dimensional model and computational requirements, we simplified the properties of the future allochthonous terranes, including their size, strength, and shape. In addition, we considered various types of future allochthonous terranes, such as microcontinents and oceanic plateaus, using the same material properties and dimensions, which is not strictly rigorous. However, if we only consider the buoyancy characteristics of the buoyant blocks and ignore the rheological characteristics, based on the results of Tetreault

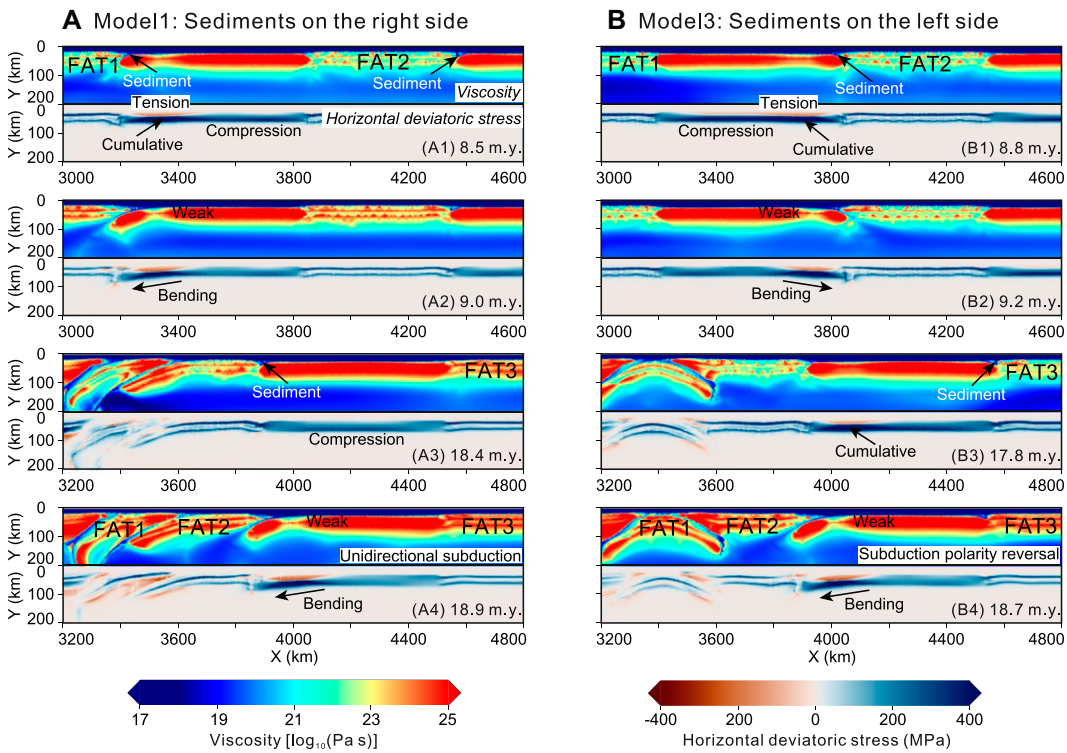

Figure 8. Comparison of models with different sediment settings. Evolution of viscosity (above) and horizontal deviatoric stress (below) in Model 1 (A) with sediments on the right side of future allochthonous terranes (FATs) and in Model 3 (B) with sediments on the left side of future allochthonous terranes. Note that compression is positive.

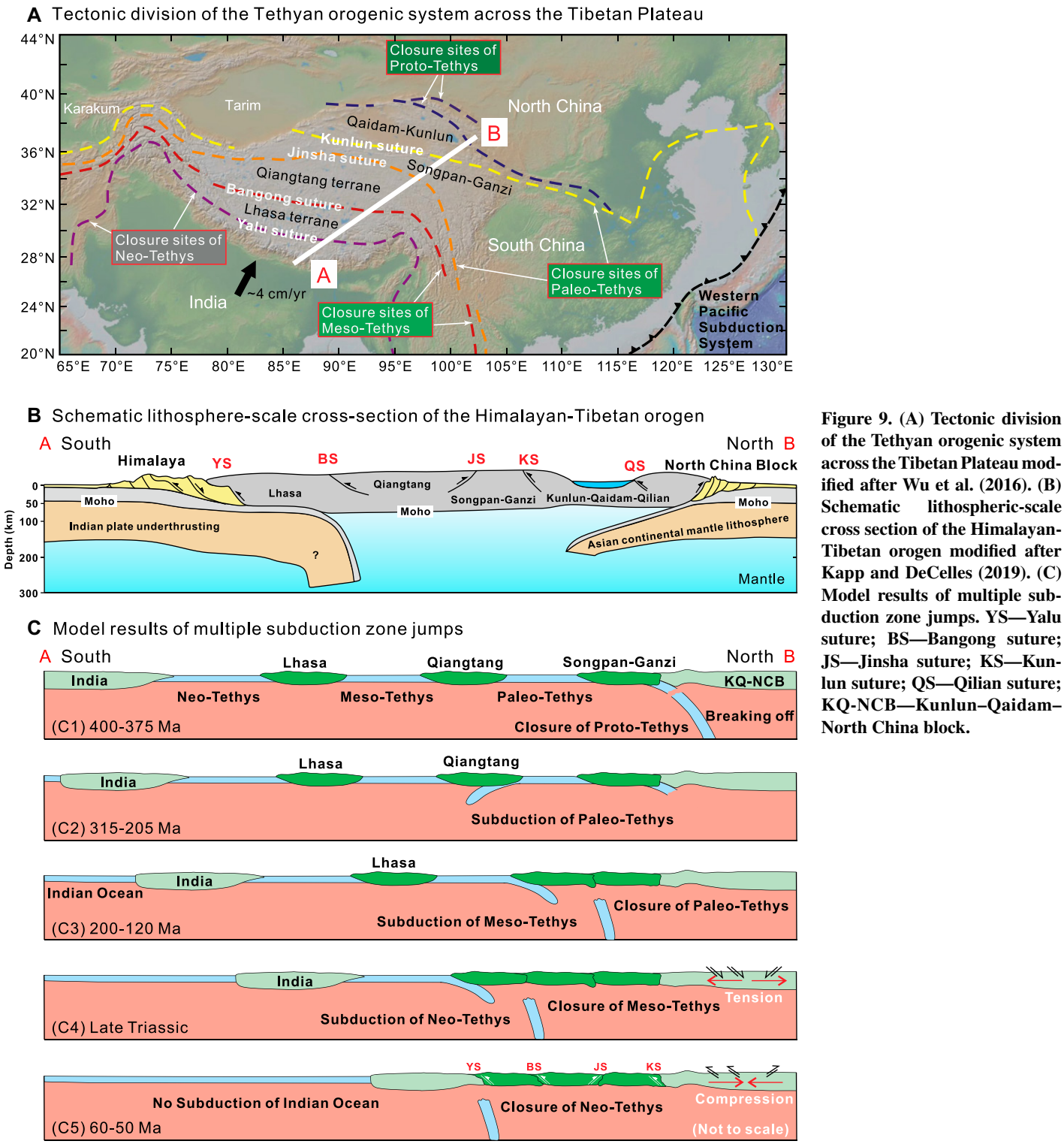

Figure 9. (A) Tectonic division of the Tethyan orogenic system across the Tibetan Plateau modified after Wu et al. (2016). (B) Schematic lithospheric-scale cross section of the Himalayan-Tibetan orogen modified after Kapp and DeCelles (2019). (C) Model results of multiple subduction zone jumps. YS—Yalu suture; BS—Bangong suture; JS—Jinsha suture; KS—Kunlun suture; QS—Qilian suture; KQ-NCB—Kunlun–Qaidam–North China block.

and Buiter (2014), it is also reasonable for us to represent these microcontinents and oceanic plateaus only as buoyant blocks (here called future allochthonous terranes). Furthermore, we simplified the velocity condition, whereas the velocity of a subducting plate may change abruptly after the collision of terranes (e.g., Martinod et al., 2005). All of the above may affect plate dynamics, and in particular terranes with different rheological properties may accrete in different ways (Vogt and Gerya, 2014), which will need to be considered in future work.

The geologic histories of the various future allochthonous terranes and oceanic plateaus are continually being reinterpreted through updated geologic investigations. Although some models emphasize the broad one-way, north-directed accretion of these terranes onto the Eurasian

TABLE 2. SUMMARY OF SUTURE ZONES, OCEANS, AND SUBDUCTION EVENTS IN TIBET

Suture	Ocean	Subduction polarity	North-moving terrane	Upper-plate block	Subduction arc activity (Ma)	Ocean closure age (Ma)	Subduction jump timing*	References
Qilian	Qilian Ocean	North-dipping	Qilian oceanic plateau	Qilian	550–430	470	10–20 m.y.	Song et al. (2017)
Kunlun	Proto-Tethyan (Paleo-Kunlun)	North-dipping	Songpan-Ganzi (Yangtze)	Kunlun-Qaidam	550–410	400–375	NA	Wu et al. (2016)
Jinsha	Paleo-Tethyan (Neo-Kunlun)	South-dipping	Qiangtang	Songpan-Ganzi (Yangtze)	315–205	200–190	>60 m.y.	Kapp et al. (2003); Kapp and DeCelles (2019); Liu et al. (2021)
Banggong	Meso-Tethyan	North-dipping	Lhasa	Qiangtang	200–120	120–110	~0–10 m.y.	Kapp and DeCelles (2019)
Banggong	Meso-Tethyan	North-dipping	Meso-Tethyan oceanic plateau	Qiangtang	200–120	175	10 m.y.	Yan and Zhang (2020)
Indus-Yarlung	Neo-Tethyan	North-dipping	India	Lhasa	Late Triassic	60–50	Active long before collision	Liu et al. (2021); Wan et al. (2019)
None	Indian Ocean	NA	NA	India	NA	NA	NA	Kapp and DeCelles (2019); Stern and Gerya (2018)

Note: NA—not applicable.
*Timing from terrane collision to new subduction initiation in the south.

continent (e.g., Wan et al., 2019), there are important complexities to this history, including subduction zones that formed prior to terrane collisions. The long-lived Gangdese arc on the southern margin of the Lhasa terrane is a notable example, where arc magmatism since ca. 230 Ma accommodated the northward subduction of the Neo-Tethyan Ocean (Table 1). This magmatism clearly initiated before the Cretaceous closure of the Meso-Tethyan Ocean to the north, and therefore this terrane-accretion event did not induce subduction to the south. That said, the modeling presented here represents an end-member scenario for testing how terrane accretion could initiate subduction-zone jumps. If a subduction system were already active before terrane collisions, this model would not be directly applicable.

Although we made several simplifications, our model results remain physically plausible. Our numerical investigation provides novel insight into the continuous collision and successive accretion of multiple future allochthonous terranes, identifies parameter characteristics that may influence multiple unidirectional subduction zone jumps, and improves our understanding of the evolution of Tethys.

6. CONCLUSIONS

We systematically examined the subduction and collision dynamics of multiple terranes. We found that multiple subduction zone jumps are possible if future allochthonous terranes are surrounded by thick sediment and oceanic subduction keeps consistent. We propose that the accretion of multiple terranes surrounded by thick sediment can be used to reproduce the process of multiple Tethyan subduction initiation and successive episodes of accretion triggered by future allochthonous terranes. We also provide a possible explanation for the long-term absence of subduction in the Indian Ocean today. Our main conclusions are as follows:

(1) Large (≥400 km) and buoyant terranes with fast continental plate motion promote subduction initiation shortly after collision, and sediments around the future allochthonous terranes help guide subduction polarity.

(2) The jumping time of multiple subduction zone jumps is ~3–20 + m.y., which is primarily controlled by the convergence rate and the continental plate composed of accreted terranes.

(3) The Indian Ocean did not show signs of subduction initiation for a long time after the India-Eurasia collision, perhaps due to slower convergence rates and the partitioning of deformation across southern Asia.

(4) We predict that in the future, the accumulation of sediments on the southern margin of India to a certain thickness and/or the action of a far-field force (oceanic ridge or mantle plume) will induce a new northward subduction of the Indian Ocean.

ACKNOWLEDGMENTS

We thank Taras Gerya for providing the I2VIS code. We thank Joya Tetreault and one anonymous reviewer for their constructive comments and suggestions, which greatly improved the presentation of the paper. We also thank the science editor, Mihai Ducea, and the associate editor, Xixi Zhao, for their excellent editorial work. All of the figures were generated with GMT (https://www.soest.hawaii.edu/gmt/) and Python (https://www.python.org/). This study was supported by National Natural Science Foundation of China grant no. 91955311 to Q. Meng, National Natural Science Foundation of China grant no. 42204099 to Z. Yan, and the U.S. National Science Foundation EAR grant nos. 1914501 and 2210074 to A. Zuza. All models were run at the Beijing Super Cloud Computing Center and at the Supercomputing Laboratory, Institute of Geology and Geophysics, Chinese Academy of Sciences, in Beijing. Data will be made available on request, and all data related to the numerical models are provided on Zenodo (https://doi.org/10.5281/zenodo.8021129).

REFERENCES CITED

Abbott, D., and Mooney, W., 1995, The structural and geochemical evolution of the continental crust: Support for the oceanic plateau model of continental growth: Reviews of Geophysics, v. 33, p. 231–242, https://doi.org/10.1029/95RG00551.

Bangs, N.L., Moore, G.F., Gulick, S.P., Pangborn, E.M., Tobin, H.J., Kuramoto, S., and Taira, A., 2009, Broad, weak regions of the Nankai Megathrust and implications for shallow coseismic slip: Earth and Planetary Science Letters, v. 284, p. 44–49, https://doi.org/10.1016/j.epsl.2009.04.026.

Behr, W.M., and Becker, T.W., 2018, Sediment control on subduction plate speeds: Earth and Planetary Science Letters, v. 502, p. 166–173, https://doi.org/10.1016/j.epsl.2018.08.057.

Brizzi, S., van Zelst, I., Funiciello, F., Corbi, F., and van Dinther, Y., 2020, How sediment thickness influences subduction dynamics and seismicity: Journal of Geophysical Research: Solid Earth, v. 125, https://doi.org/10.1029/2019JB018964.

Chen, L., Capitanio, F.A., Liu, L., and Gerya, T.V., 2017, Crustal rheology controls on the Tibetan plateau formation during India-Asia convergence: Nature Communications, v. 8, p. 15,992–15,998, https://doi.org/10.1038/ncomms15992.

Chen, L., Liu, L., Capitanio, F.A., Gerya, T.V., and Li, Y., 2020, The role of pre-existing weak zones in the formation of the Himalaya and Tibetan plateau: 3-D thermomechanical modelling: Geophysical Journal International, v. 221, p. 1971–1983, https://doi.org/10.1093/gji/ggaa125.

Clark, M.K., 2012, Continental collision slowing due to viscous mantle lithosphere rather than topography: Nature, v. 483, p. 74–77, https://doi.org/10.1038/nature10848.

Cloetingh, S., Wortel, R., and Vlaar, N.J., 1982, Evolution of passive continental margins and initiation of subduction zones: Nature, v. 297, p. 139–142, https://doi.org/10.1038/297139a0.

Cloetingh, S., Wortel, R., and Vlaar, N.J., 1989, On the initiation of subduction zones: Pure and Applied Geophysics, v. 129, p. 7–25, https://doi.org/10.1007/BF00874622.

Cloos, M., 1993, Lithospheric buoyancy and collisional orogenesis: Subduction of oceanic plateaus, continental margins, island arcs, spreading ridges, and seamounts: Geological Society of America Bulletin, v. 105, p. 715–737, https://doi.org/10.1130/0016-7606(1993)105<0715:LBACOS>2.3.CO;2.

Copley, A., Avouac, J.P., and Royer, J.Y., 2010, India-Asia collision and the Cenozoic slowdown of the Indian plate: Implications for the forces driving plate motions: Journal of Geophysical Research: Solid Earth, v. 115, https://doi.org/10.1029/2009JB006634.

DeCelles, P.G., Kapp, P., Gehrels, G.E., and Ding, L., 2014, Paleocene–Eocene foreland basin evolution in the Himalaya of southern Tibet and Nepal: Implications for

the age of initial India-Asia collision: Tectonics, v. 33, p. 824–849, https://doi.org/10.1002/2014TC003522.

Gerya, T.V., and Meilick, F.I., 2011, Geodynamic regimes of subduction under an active margin: Effects of rheological weakening by fluids and melts: Journal of Metamorphic Geology, v. 29, p. 7–31, https://doi.org/10.1111/j.1525-1314.2010.00904.x.

Gerya, T.V., and Yuen, D.A., 2003, Characteristics-based marker-in-cell method with conservative finite-differences schemes for modeling geological flows with strongly variable transport properties: Physics of the Earth and Planetary Interiors, v. 140, p. 293–318, https://doi.org/10.1016/j.pepi.2003.09.006.

Gün, E., Pysklywec, R.N., Göğüş, O.H., and Topuz, G., 2021, Pre-collisional extension of microcontinental terranes by a subduction pulley: Nature Geoscience, v. 14, p. 443–450, https://doi.org/10.1038/s41561-021-00746-9.

Hoareau, G., Bomou, B., van Hinsbergen, D.J.J., Carry, N., Marquer, D., Donnadieu, Y., Le Hir, G., Vrielynck, B., and Walter-Simonnet, A.-V., 2015, Did high Neo-Tethys subduction rates contribute to early Cenozoic warming?: Climate of the Past, v. 11, p. 1751–1767, https://doi.org/10.5194/cp-11-1751-2015.

Ingalls, M., Rowley, D.B., Currie, B., and Colman, A.S., 2016, Large-scale subduction of continental crust implied by India-Asia mass-balance calculation: Nature Geoscience, v. 9, p. 848–853, https://doi.org/10.1038/ngeo2806.

Kapp, P., and DeCelles, P.G., 2019, Mesozoic–Cenozoic geological evolution of the Himalayan-Tibetan orogen and working tectonic hypotheses: American Journal of Science, v. 319, p. 159–254, https://doi.org/10.2475/03.2019.01.

Kapp, P., Yin, A., Manning, C.E., Harrison, T.M., Taylor, M.H., and Ding, L., 2003, Tectonic evolution of the early Mesozoic blueschist-bearing Qiangtang metamorphic belt, central Tibet: Tectonics, v. 22, https://doi.org/10.1029/2002TC001383.

Kerr, A.C., 2014, Oceanic plateaus, *in* Turekian, K.K., and Holland, H.D., eds., Treatise on Geochemistry (second edition): Oxford, UK, Elsevier, p. 631–667, https://doi.org/10.1016/B978-0-08-095975-7.00320-X.

Kiss, D., Candioti, L., Duretz, T., and Schmalholz, S., 2020, Thermal softening induced subduction initiation at a passive margin: Geophysical Journal International, v. 220, p. 2068–2073, https://doi.org/10.1093/gji/ggz572.

Kopf, A., and Brown, K.M., 2003, Friction experiments on saturated sediments and their implications for the stress state of the Nankai and Barbados subduction thrusts: Marine Geology, v. 202, p. 193–210, https://doi.org/10.1016/S0025-3227(03)00286-X.

Lallemand, S., Heuret, A., and Boutelier, D., 2005, On the relationships between slab dip, back-arc stress, upper plate absolute motion, and crustal nature in subduction zones: Geochemistry, Geophysics, Geosystems, v. 6, https://doi.org/10.1029/2005GC000917.

Leng, W., and Gurnis, M., 2015, Subduction initiation at relic arcs: Geophysical Research Letters, v. 42, p. 7014–7021, https://doi.org/10.1002/2015GL064985.

Li, B., Zuza, A.V., Chen, X., Hu, D., Shao, Z., Qi, B., and Wang, Z., 2020, Cenozoic multi-phase deformation in the Qilian Shan and out-of-sequence development of the northern Tibetan Plateau: Tectonophysics, v. 782–783, https://doi.org/10.1016/j.tecto.2020.228423.

Li, Z., Cui, F., Yang, S., and Zhong, X., 2023, Key geodynamic processes and driving forces of Tethyan evolution: Science China Earth Sciences, v. 66, https://doi.org/10.1007/s11430-022-1083-5.

Liu, J.L., Chen, X.Y., Fan, W.K., Shan, H.S., Yan, J.X., Ding, X., and Zhao, T., 2021, Dynamics of closure of the Proto-Tethys Ocean: A perspective from the southeast Asian Tethys realm: Earth-Science Reviews, v. 222, https://doi.org/10.1016/j.earscirev.2021.103829.

Liu, L., Liu, L., Morgan, J.P., Xu, Y.G., and Chen, L., 2023, New constraints on Cenozoic subduction between India and Tibet: Nature Communications, v. 14, 1963, https://doi.org/10.1038/s41467-023-37615-5.

Marques, F., Nikolaeva, K., Assumpcao, M., Gerya, T., Bezerra, F., do Nascimento, A., and Ferreira, J., 2013, Testing the influence of far-field topographic forcing on subduction initiation at a passive margin: Tectonophysics, v. 608, p. 517–524, https://doi.org/10.1016/j.tecto.2013.08.035.

Marques, F., Cabral, F., Gerya, T., Zhu, G., and May, D., 2014, Subduction initiates at straight passive margins: Geology, v. 42, p. 331–334, https://doi.org/10.1130/G35246.1.

Martinod, J., Funiciello, F., Faccenna, C., Labanieh, S., and Regard, V., 2005, Dynamical effects of subducting ridges: Insights from 3-D laboratory models: Geophysical Journal International, v. 163, p. 1137–1150, https://doi.org/10.1111/j.1365-246X.2005.02797.x.

Mochizuki, K., Sutherland, R., Henrys, S., Bassett, D., Van Avendonk, H., Arai, R., and Kodaira, S., 2019, Recycling of depleted continental mantle by subduction and plumes at the Hikurangi Plateau large igneous province, southwestern Pacific Ocean: Geology, v. 47, p. 795–798, https://doi.org/10.1130/G46250.1.

Molnar, P., and Stock, J.M., 2009, Slowing of India's convergence with Eurasia since 20 Ma and its implications for Tibetan mantle dynamics: Tectonics, v. 28, https://doi.org/10.1029/2008TC002271.

Moresi, L., Betts, P., Miller, M., and Cayley, R.A., 2014, Dynamics of continental accretion: Nature, v. 508, p. 245–248, https://doi.org/10.1038/nature13033.

Nikolaeva, K., Gerya, T., and Marques, F., 2010, Subduction initiation at passive margins: Numerical modeling: Journal of Geophysical Research: Solid Earth, v. 115, https://doi.org/10.1029/2009JB006549.

Nikolaeva, K., Gerya, T., and Marques, F., 2011, Numerical analysis of subduction initiation risk along the Atlantic American passive margins: Geology, v. 39, p. 463–466, https://doi.org/10.1130/G31972.1.

Niu, Y., 2018, Geological understanding of plate tectonics: Basic concepts, illustrations, examples and new perspectives: Global Tectonics and Metallogeny, v. 10, p. 23–46, https://doi.org/10.1127/gtm/2014/0009.

Scott, J.M., Waight, T.E., van der Meer, Q.H.A., Palin, J.M., Cooper, A.F., and Munker, C., 2014, Metasomatized ancient lithospheric mantle beneath the young Zealandia microcontinent and its role in HIMU-like intraplate magmatism: Geochemistry, Geophysics, Geosystems, v. 15, p. 3477–3501, https://doi.org/10.1002/2014GC005300.

Sebastian, T., Nath, B.N., Ramaswamy, V., Mascarenhas-Pereira, M.B.L., Yazing, A.K., Apurva, P.R., Linsy, P., Kocherla, M., Miriyala, P., and Rao, B.R., 2019, Distribution and dispersal of surface sediments on the continental margins of India: Marine and Petroleum Geology, v. 110, p. 122–137, https://doi.org/10.1016/j.marpetgeo.2019.07.017.

Şengör, A.M.C., Altıner, D., Cin, A., Ustaömer, T., and Hsü, K.J., 1988, Origin and assembly of the Tethyside orogenic collage at the expense of Gondwana-land, *in* Audley-Charles, M.G., and Hallam, A., eds., Gondwana and Tethys: Geological Society, London, Special Publication 37, p. 119–181, https://doi.org/10.1144/GSL.SP.1988.037.01.09.

Şengör, A.M.C., Natal'in, B.A., Sunal, G., and van der Voo, R., 2018, The tectonics of the Altaids: Crustal growth during the construction of the continental lithosphere of Central Asia between ~750 and ~130 Ma ago: Annual Review of Earth and Planetary Sciences, v. 46, p. 439–494, https://doi.org/10.1146/annurev-earth-060313-054826.

Song, S.G., Yang, L.M., Zhang, Y.Q., Niu, Y.L., Wang, C., Su, L., and Gao, Y.L., 2017, Qi-Qin accretionary belt in Central China Orogen: Accretion by trench jam of oceanic plateau and formation of intra-oceanic arc in the early Paleozoic Qin-Qi-Kun Ocean: Science Bulletin, v. 62, p. 1035–1038, https://doi.org/10.1016/j.scib.2017.07.009.

Song, S.G., Bi, H., Qi, S., Yang, L., Allen, M.B., Niu, Y., Su, L., and Li, W., 2018, HP-UHP metamorphic belt in the East Kunlun Orogen: Final closure of the Proto-Tethys Ocean and formation of the Pan-North-China Continent: Journal of Petrology, v. 59, p. 2043–2060, https://doi.org/10.1093/petrology/egy089.

Stampfli, G.M., and Borel, G.D., 2002, A plate tectonic model for the Paleozoic and Mesozoic constrained by dynamic plate boundaries and restored synthetic oceanic isochrons: Earth and Planetary Science Letters, v. 196, p. 17–33, https://doi.org/10.1016/S0012-821X(01)00588-X.

Stern, R.J., 2004, Subduction initiation: Spontaneous and induced: Earth and Planetary Science Letters, v. 226, p. 275–292, https://doi.org/10.1016/S0012-821X(04)00498-4.

Stern, R.J., and Gerya, T.V., 2018, Subduction initiation in nature and models: A review: Tectonophysics, v. 746, p. 173–198, https://doi.org/10.1016/j.tecto.2017.10.014.

Sun, B., Kaus, B.J., Yang, J., Lu, G., Wang, X., Wang, K., and Zhao, L., 2021, Subduction polarity reversal triggered by oceanic plateau accretion: Implications for induced subduction initiation: Geophysical Research Letters, v. 48, https://doi.org/10.1029/2021GL095299.

Tao, J., Dai, L., Lou, D., Li, Z., Zhou, S., Liu, Z., and Li, S., 2020, Accretion of oceanic plateaus at continental margins: Numerical modeling: Gondwana Research, v. 81, p. 390–402, https://doi.org/10.1016/j.gr.2019.11.015.

Tetreault, J.L., and Buiter, S.J.H., 2012, Geodynamic models of terrane accretion: Testing the fate of island arcs, oceanic plateaus, and continental fragments in subduction zones: Journal of Geophysical Research: Solid Earth, v. 117, https://doi.org/10.1029/2012JB009316.

Tetreault, J.L., and Buiter, S.J.H., 2014, Future accreted terranes: A compilation of island arcs, oceanic plateaus, submarine ridges, seamounts, and continental fragments: Journal of Geophysical Research: Solid Earth, v. 5, p. 1243–1275, https://doi.org/10.5194/sed-6-1451-2014.

Tobin, H.J., and Saffer, D.M., 2009, Elevated fluid pressure and extreme mechanical weakness of a plate boundary thrust, Nankai Trough subduction zone: Geology, v. 37, p. 679–682, https://doi.org/10.1130/G25752A.1.

Vogt, K., and Gerya, T.V., 2014, From oceanic plateaus to allochthonous terranes: Numerical modelling: Gondwana Research, v. 25, p. 494–508, https://doi.org/10.1016/j.gr.2012.11.002.

Wan, B., Wu, F.Y., Chen, L., Zhao, L., Liang, X.F., Xiao, W.J., and Zhu, R.X., 2019, Cyclical one-way continental rupture-drift in the Tethyan evolution: Subduction-driven plate tectonics: Science China: Earth Sciences, v. 62, p. 2005–2016, https://doi.org/10.1007/s11430-019-9393-4.

Wang, L., and Barbot, S., 2023, Three-dimensional kinematics of the India-Eurasia collision: Communications Earth & Environment, v. 4, https://doi.org/10.1038/s43247-023-00815-4.

Wang, Y., Chen, X.H., Zhang, Y.Y., Yin, Z., Zuza, A.V., Yin, A., Wang, Y.C., Ding, W.C., Xu, S.L., Zhang, Y.P., Li, B., and Shao, Z.G., 2022, Superposition of Cretaceous and Cenozoic deformation in northern Tibet: A far-field response to the tectonic evolution of the Tethyan orogenic system: Geological Society of America Bulletin, v. 134, p. 501–525, https://doi.org/10.1130/B35944.1.

Wu, C., Yin, A., Zuza, A.V., Zhang, J., Liu, W., and Ding, L., 2016, Pre-Cenozoic geologic history of the central and northern Tibetan Plateau and the role of Wilson cycles in constructing the Tethyan orogenic system: Lithosphere, v. 8, p. 254–292, https://doi.org/10.1130/L494.1.

Wu, F.Y., Wan, B., Zhao, L., Xiao, W.J., and Zhu, R.X., 2020, Tethyan geodynamics: Acta Petrologica Sinica (Yanshi Xuebao), v. 36, p. 1627–1674, https://doi.org/10.18654/1000-0569/2020.06.01.

Xie, R., Chen, L., Xiong, X., Wang, K., and Yan, Z., 2021, The role of pre-existing crustal weaknesses in the uplift of the eastern Tibetan Plateau: 2D thermomechanical modeling: Tectonics, v. 40, https://doi.org/10.1029/2020TC006444.

Yakovlev, P.V., and Clark, M.K., 2014, Conservation and redistribution of crust during the Indo-Asian collision: Tectonics, v. 33, p. 1016–1027, https://doi.org/10.1002/2013TC003469.

Yan, L.L., and Zhang, K.J., 2020, Infant intra-oceanic arc magmatism due to initial subduction induced by oceanic plateau accretion: A case study of the Bangong Meso-Tethys, central Tibet, western China: Gondwana Research, v. 79, p. 110–124, https://doi.org/10.1016/j.gr.2019.08.008.

Yan, Z., Chen, L., Xiong, X., Wan, B., and Xu, H., 2021, Oceanic plateau and subduction zone jump: Two-

dimensional thermomechanical modeling: Journal of Geophysical Research: Solid Earth, v. 126, https://doi.org/10.1029/2021JB021855.

Yan, Z., Chen, L., Zuza, A.V., Tang, J., Wan, B., and Meng, Q., 2022, The fate of oceanic plateaus: Subduction versus accretion: Geophysical Journal International, v. 231, p. 1349–1362, https://doi.org/10.1093/gji/ggac266.

Yang, G., 2022, Subduction initiation triggered by collision: A review based on examples and models: Earth-Science Reviews, v. 232, https://doi.org/10.1016/j.earscirev.2022.104129.

Yin, A., and Harrison, T.M., 2000, Geologic evolution of the Himalayan-Tibetan orogen: Annual Review of Earth and Planetary Sciences, v. 28, p. 211–280, https://doi.org/10.1146/annurev.earth.28.1.211.

Zhang, W.Q., Liu, C.Z., Liu, T., Zhang, C., and Zhang, Z.Y., 2021, Subduction initiation triggered by accretion of a Jurassic oceanic plateau along the Bangong-Nujiang Suture in central Tibet: Terra Nova, v. 33, p. 150–158, https://doi.org/10.1111/ter.12500.

Zhong, X.Y., and Li, Z.H., 2020, Subduction initiation during collision-induced subduction transference: Numerical modeling and implications for the Tethyan evolution: Journal of Geophysical Research: Solid Earth, v. 125, https://doi.org/10.1029/2019JB019288.

Zhong, X.Y., and Li, Z.H., 2022, Wedge-shaped Southern Indian continental margin without proper weakness hinders subduction initiation: Geochemistry, Geophysics, Geosystems, v. 23, https://doi.org/10.1029/2021GC009998.

Zuza, A.V., Wu, C., Reith, R., Yin, A., Li, J., Zhang, J., and Zhang, Y., 2018, Tectonic evolution of the Qilian Shan: An early Paleozoic orogen reactivated in the Cenozoic: Geological Society of America Bulletin, v. 130, p. 881–925, https://doi.org/10.1130/B31721.1.

Zuza, A.V., Wu, C., Wang, Z., Levy, D.A., Li, B., Xiong, X., and Chen, X., 2019, Underthrusting and duplexing beneath the northern Tibetan Plateau and the evolution of the Himalayan-Tibetan orogen: Lithosphere, v. 11, p. 209–231, https://doi.org/10.1130/L1042.1.

Zuza, A.V., Gavillot, Y., Haproff, P.J., and Wu, C., 2020, Kinematic evolution of a continental collision: Constraining the Himalayan-Tibetan orogen via bulk strain rates: Tectonophysics, v. 797, https://doi.org/10.1016/j.tecto.2020.228642.

Science Editor: Mihai Ducea
Associate Editor: Xixi Zhao

Manuscript Received 27 July 2023
Revised Manuscript Received 31 October 2023
Manuscript Accepted 27 November 2023